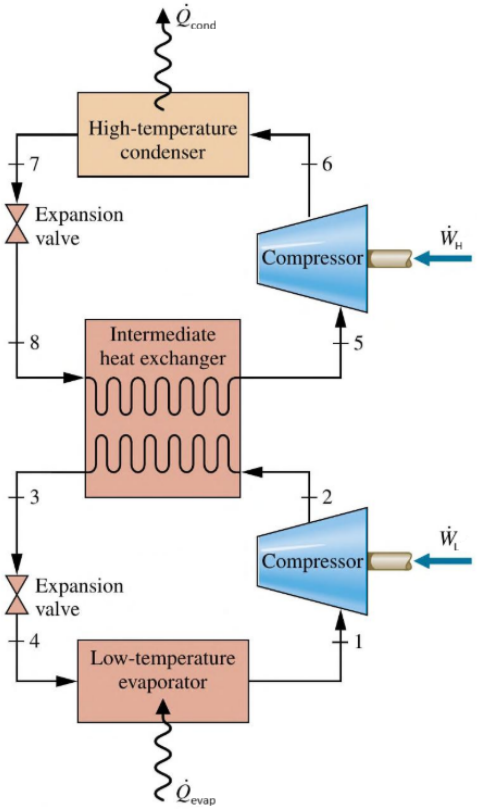

Modeling and Control System Design of a Cascade Vapor Compression System

Master's thesis in Complex Adaptive Systems

CASPER JARHULT

DEPARTMENT OF PHYSICS

CHALMERS UNIVERSITY OF TECHNOLOGY
Gothenburg, Sweden 2025
www.chalmers.se

Master's thesis 2025

Modeling and Control System Design of a Cascade Vapor Compression System

CASPER JARHULT

CHALMERS
UNIVERSITY OF TECHNOLOGY

Department of Physics
Chalmers University of Technology
Gothenburg, Sweden 2025

Modeling and Control System Design of a Cascade Vapor Compression System
CASPER JARHULT

Supervisor: Olof Hannius, GKN Aerospace Sweden AB
Examiner: Magnus Karlsteen, Department of Physics

Master's Thesis 2025
Department of Physics
Chalmers University of Technology
SE-412 96 Gothenburg
Telephone +46 31 772 1000

Cover: Model of a cascade vapor compression system [1].

Typeset in LaTeX
Printed by Chalmers Reproservice
Gothenburg, Sweden 2025

Modeling and Control System Design of a Cascade Vapor Compression System
CASPER JARHULT
Department of Physics
Chalmers University of Technology

Abstract

This thesis investigates the modeling, simulation, and analysis of a cascade vapor compression system designed for aerospace thermal management, delivering a 25 kW cooling capacity. Control design focuses on maintaining a liquid coolant at 20 °C, ensuring 5 °C superheat at the evaporator outlets, and an intermediate temperature set to the geometric mean of the low-stage evaporator and high-stage condenser to enhance system efficiency. PI controllers are incorporated to regulate performance under various operating conditions. A MATLAB Simscape model was developed using R134a for the low stage and R1233zd(E) for the high stage, enabling performance evaluation across a range of ambient temperatures and heat loads. Simulations demonstrate that the cascade configuration can maintain stable coolant temperatures across a wide range of ambient conditions, as well as sufficient superheat at the evaporator outlets. The use of the geometric mean for selecting the intermediate pressure ratio proved effective, though not optimal, as evidenced by variations in compressor power input between the low- and high-stage cycles. However, limitations were identified at low ambient temperatures, where evaporator and condenser pressures converge, causing instability in superheat control. Additional challenges were observed at low heat loads, where controller performance was sensitive to tuning, resulting in oscillations. These results demonstrate the viability of cascade vapor compression systems for demanding aerospace thermal management tasks, while highlighting challenges related to low-temperature operation and controller robustness that require further investigation.

Keywords: Vapor Compression System, Cascade System, Refrigeration, Simulink, Simscape.

Acknowledgements

I would like to thank Olof Hannius and Erik Hartelius for their inputs and guidance throughout the master thesis. I would also like to thank everyone on the Controls department at GKN for making me feel like part of the team. Lastly, I would like to thank my examiner Magnus Karlsteen at Chalmers University of Technology.

Casper Jarhult, Gothenburg, September 2025

List of Acronyms

Below is the list of acronyms that have been used throughout this thesis listed in alphabetical order:

2P	Two-Phase
COP	Coefficient of Performance
GKN	GKN Aerospace Sweden AB
HS	High-Stage Cycle
LS	Low-Stage Cycle
VCS	Vapor Compression System

Nomenclature

Below is the nomenclature of indices, sets, parameters, and variables that have been used throughout this thesis.

Indices

$comp$	Compressor
$cond$	Condenser
$evap$	Evaporator
h	High-stage
in	Inlet
$cool$	Liquid coolant
l	Low-stage
out	Outlet
pro	Process value
ref	Refrigerant
sat	Saturated

Variables

D_{SC}	Degree of subcooling
D_{SH}	Degree of superheat
$\dot{Q}$	Rate of heat flow
$\dot{m}$	Rate of mass flow
T	Temperature
h	Specific enthalpy
p	Pressure
c_p	Specific heat

Contents

List of Figures

1

Introduction

The aerospace industry plays an essential role in the advancement of technology, driven by the need for better performance, efficiency, and sustainability in modern aircraft. GKN Aerospace, a global leader in aerospace manufacturing, operates 55 facilities across 15 countries, serving over 90% of the world's aircraft and engine manufacturers with advanced systems and components for platforms ranging from commercial airliners to fighter jets and the European Space Agency's Ariane rockets.

Modern aircraft integrate complex systems, including advanced avionics, propulsion technologies, and electric power systems, which generate substantial and dynamic heat loads. These loads vary across the flight envelope due to changes in operating conditions such as altitude, airspeed, and mission profiles. External environmental factors, including ambient temperature fluctuations influenced by aerodynamic effects like friction and turbulence, further complicate heat rejection. Effective thermal management is critical to ensure the reliability and efficiency of aircraft components under these conditions.

Traditional cooling methods, such as air-cycle systems, face limitations in meeting these demands. Air-cycle systems, commonly used for cabin and avionics cooling, rely on compressed air from engine bleed or auxiliary power units, expanded through turbines to produce cooling. Although lightweight and reliable, they exhibit reduced efficiency at high altitudes and under variable heat loads, increasing fuel consumption [2].

Vapor compression systems (VCS) offer a promising alternative. Modern aircraft, such as the Boeing 787 and Airbus A380, increasingly incorporate VCS as auxiliary cooling units to enhance onboard thermal management. In the Boeing 787, a VCS module provides 35 kW of cooling capacity for galleys while supporting cabin air conditioning through subcooling, utilizing a quasi-two-stage cycle with a 76 kg unit. Similarly, the Airbus A380 employs a VCS to cool galleys, drinking water, and electronic equipment, featuring a single-stage cycle with a rolling rotor compressor, delivering 15 kW of cooling via aluminum alloy plate-fin heat exchangers, with each cooling unit weighing 83 kg. These applications highlight the critical role of VCS in achieving efficient and reliable refrigeration in advanced aircraft systems, setting the stage for this thesis to explore their design and performance optimization [3].

1.1 Aim

The primary aim of this thesis is to investigate the performance and control of a two-stage cascade VCS, assessing its ability to meet cooling demands under varying operating conditions. This involves constructing a model of the VCS that incorporates realistic thermodynamics and heat transfer dynamics to simulate the thermal management of a liquid coolant with a 25 kW cooling capacity at an ambient temperature of 100°C. The study seeks to identify key system variables essential for monitoring and controlling system stability and performance. Additionally, it aims to develop a control strategy that enables the VCS to adapt to changing operating conditions, ensuring rapid response and robust operation. The system's performance will be evaluated under diverse conditions, including variations in ambient temperature and heat load. The findings are intended to support GKN's mission of driving innovation in efficient thermal management systems for next-generation aerospace applications.

1.2 Limitations

The scope of this study is limited to the simulation and analysis of a cascade VCS to characterize its behavior and control requirements. Detailed design and optimization of individual components, such as compressors, heat exchangers, or expansion valves, are outside the scope of this thesis. The model employs idealized component representations, prioritizing system-level performance over hardware-specific details. Physical constraints such as weight, size or material properties, critical for practical aircraft integration, are not considered. Additionally, environmental impacts, such as refrigerant leakage or gravitational effects, are beyond the scope of this work.

2

Theory

This chapter presents the theoretical foundation of vapor compression systems. Section 2.1 introduces the principles of vapor compression systems, including their components, thermodynamic performance measures, refrigerant selection and control strategies. Section 2.2 extends this discussion to two-stage cascade systems, describing their advantages over single-stage cycles, the role of intermediate temperature and heat exchanger design, and the control strategies required for performance optimization.

2.1 Principles of Vapor Compression Systems

The vapor compression system (VCS) is a fundamental technology in modern refrigeration and heat pump applications, widely used for its efficiency in transferring heat from a low-temperature source to a higher-temperature sink [1][5]. The system operates by circulating a refrigerant through a closed-loop cycle, leveraging phase changes to facilitate heat transfer.

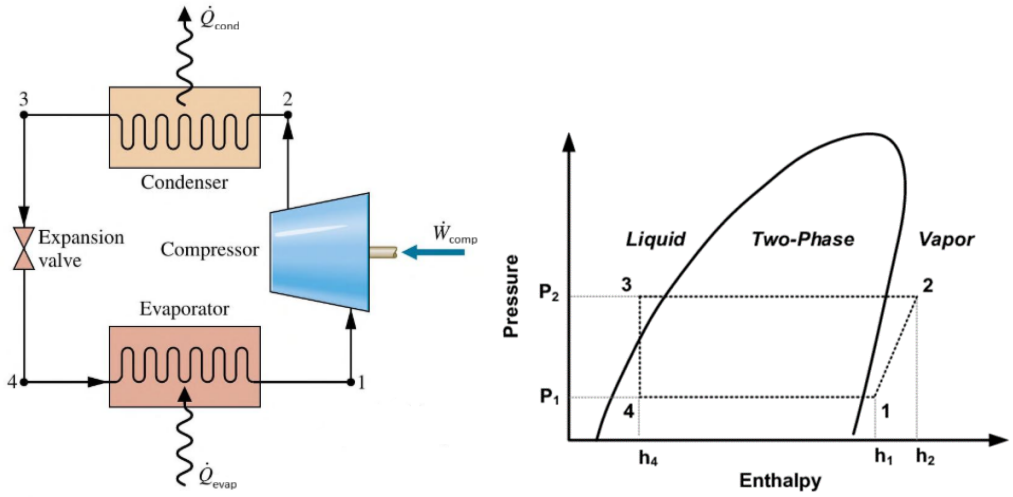

Figure 2.1: VCS and corresponding points in a p-h diagram [1][4].

A VCS comprises four primary components: the evaporator, compressor, condenser, and expansion device. Figure 2.1 illustrates the main components of a single-stage VCS with a corresponding pressure-enthalpy (p-h) diagram.

- **Evaporator** — In the evaporator, low-pressure liquid refrigerant absorbs heat, Q_{evap}, from a higher-temperature refrigerated space. The refrigerant undergoes a phase change to saturated or slightly superheated vapor, providing the cooling effect. The absorbed heat is calculated as:

$$\dot{Q}_{evap} = \dot{m}(h_1 - h_4), \tag{2.1}$$

  where $\dot{m}$ is the refrigerant mass flow rate, h_1 is the enthalpy at the evaporator outlet, and h_4 is the enthalpy at the evaporator inlet [1].
- **Compressor** — The vapor enters the compressor, where its pressure and temperature are increased. The required compressor power, $\dot{W}_{comp}$, is expressed as:

$$\dot{W}_{comp} = \dot{m}(h_2 - h_1), \tag{2.2}$$

  where h_2 is the enthalpy at the compressor outlet. Although compression is ideally isentropic, real systems experience inefficiencies due to frictional losses and heat dissipation [1].
- **Condenser** — The high-pressure vapor flows into the condenser, where heat, Q_{cond}, is released to a lower-temperature sink, such as ambient air or cooling water. The refrigerant condenses into a saturated or subcooled liquid, and the rejected heat is given by:

$$\dot{Q}_{cond} = \dot{m}(h_2 - h_3), \tag{2.3}$$

  where h_3 is the enthalpy at the condenser outlet [1].
- **Expansion Device** — The high-pressure liquid refrigerant passes through an expansion device, where it undergoes isenthalpic expansion:

$$h_3 = h_4. \tag{2.4}$$

  The resulting low-pressure mixture re-enters the evaporator, completing the cycle [1].

The coefficient of performance (COP) for a refrigeration system is defined as:

$$COP = \frac{\dot{Q}_{evap}}{\dot{W}_{comp}} = \frac{h_1 - h_4}{h_2 - h_1}, \tag{2.5}$$

serving as a key measure of the system's efficiency, relating the cooling capacity to the power input for the system [5].

2.1.1 Degree of Superheat

At the evaporator outlet, the refrigerant is typically maintained in a slightly superheated state to ensure that only vapor enters the compressor, preventing wet compression that could damage compressor components [1]. The degree of superheat is defined as:

$$D_{\mathrm{SH}} = T_{evap,out} - T_{evap,sat}, \tag{2.6}$$

where $T_{evap,out}$ is the refrigerant temperature at the evaporator outlet, and $T_{evap,sat}$ is the saturation temperature at the evaporator pressure. While maintaining some degree of superheat ensures compressor safety, excessive superheating has been shown to reduce the COP and cooling capacity by decreasing the heat absorption in the evaporator [6][7].

2.1.2 Degree of Subcooling

Subcooling occurs when the refrigerant at the condenser outlet is cooled below its saturation temperature at the given pressure. It is defined as:

$$D_{\mathrm{SC}} = T_{cond,sat} - T_{cond,out}, \tag{2.7}$$

where $T_{cond,sat}$ is the saturation temperature at the condenser pressure, and $T_{cond,out}$ is the refrigerant temperature at the condenser outlet [1]. Subcooling increases the cooling capacity and COP by allowing the refrigerant to absorb more heat in the evaporator before reaching saturation. However, no universal optimum exists since performance depends on system design and operating conditions [6][7]. The degree of subcooling is controlled through the amount of refrigerant charged into the system [1].

2.1.3 Evaporating and Condensing Temperature

The condensing temperature is mainly influenced by the entering temperature and flow rate of the secondary fluid in the condenser. Higher secondary fluid temperatures reduce the condenser's heat transfer effectiveness, leading to increased condensing temperatures. Conversely, increasing the secondary fluid flow rate enhances heat transfer and decreases condensing temperature. Similarly, the evaporating temperature is affected by the source temperature of the system. A higher evaporating temperature results in improved COP, whereas a lower evaporating temperature reduces efficiency [6][8].

2.1.4 Refrigerant Selection Criteria

Refrigerant selection plays a critical role in determining VCS performance, safety, and environmental compliance. Several factors influence refrigerant choice. The evaporator pressure should remain above atmospheric pressure to prevent air ingress, which can degrade efficiency and cause corrosion [5]. Thermodynamic performance is also a key consideration; refrigerants with favorable enthalpy changes during phase transitions improve both the COP and cooling capacity.

2.1.5 Control Strategies for Vapor Compression Systems

Effective control strategies are crucial for optimizing VCS performance, especially in environments where dynamic thermal loads exist. Two primary mechanisms are typically used: the expansion valve restriction and the compressor mass flow. In modern systems, the expansion valve is often an electronic expansion valve (EEV),

which regulates the refrigerant flow into the evaporator and directly influences the degree of superheat. A more restricted valve opening leads to a lower evaporator pressure, which subsequently increases superheat. The compressor also plays a vital role by controlling the refrigerant mass flow rate and pressure ratio, which dictate the evaporator's cooling capacity. By varying the compressor speed, the system can dynamically adjust its cooling capacity to match changes in the thermal load, thereby improving COP [9].

2.2 Two-Stage Systems

Single-stage VCSs face performance limitations when large temperature differences between the evaporator and condenser temperatures are required. These challenges include high pressure ratios, which decrease volumetric efficiency and increase compressor discharge temperatures, resulting in mechanical stress and lower COP [1].

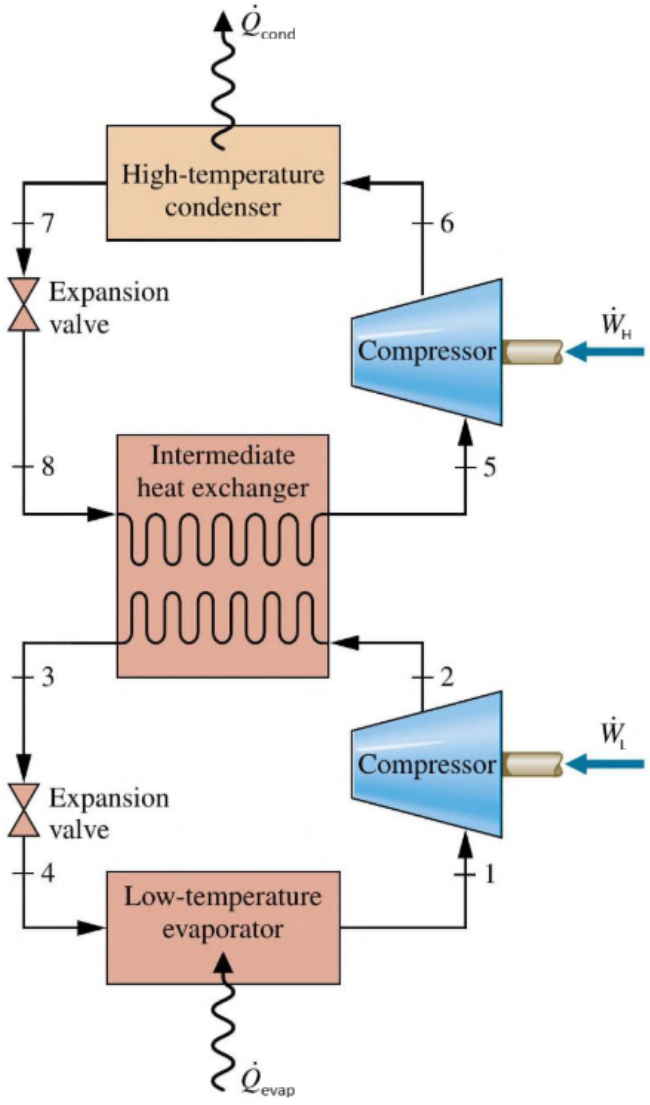

Figure 2.2: Visualization of a two-stage cascade VCS [1].

To address these challenges, multi-stage systems are implemented, which divides the total temperature and pressure lift across multiple stages. One such system is the cascade VCS, connecting two or more single-stage systems by heat exchangers, allowing each stage to use different refrigerants. For a two-stage system, the low-stage (LS) condenser rejects heat directly to the high-stage (HS) evaporator, thereby reducing compressor work per stage and improving overall efficiency [1]. Figure 2.2 shows a schematic of a typical two-stage cascade VCS.

2.2.1 Intermediate Temperature

The intermediate temperature between the LS and HS cycles significantly affects the system COP, as it influences the pressure ratios and isentropic efficiencies of the compressors. Kim et al. [10] define the intermediate temperature as the arithmetic mean of the HS evaporating temperature and LS condensing temperature. Jeong and Smith [11] found that the geometric mean of the LS evaporating temperature and HS condensing temperature yields an optimal intermediate temperature, as it minimizes entropy generation and balances temperature ratios across stages. Their analysis, however, neglects the impact of heat exchanger losses and the difference in efficiencies between the two cycles. Kim et al. [10] found that the optimal intermediate temperature that maximizes COP for a fixed operating point also depends on the Carnot efficiencies of the LS and HS, as well as the temperature difference in the heat exchanger.

2.2.2 Temperature Difference in the Cascade Heat Exchanger

The temperature difference across the cascade heat exchanger, defined as the difference between the LS condensing temperature and the HS evaporating temperature, plays an important role in determining COP. Increasing the size of the cascade heat exchanger reduces this temperature difference, improving system performance by enhancing thermal coupling between the stages. However, larger heat exchangers come with increased costs, size, and design complexity, requiring a balance between efficiency gains and practical constraints [7][8].

2.2.3 Evaporating and Condensing Temperatures in Cascade Systems

The LS condensing temperature directly affects the intermediate temperature. Raising the LS condensing temperature increases the COP of the HS cycle but decreases both the COP and cooling capacity of the LS cycle. Similarly, the HS evaporating temperature strongly impacts the mass flow ratio and COP of the system. Increasing the HS evaporating temperature improves performance up to a critical point, beyond which COP and efficiency decline [8].

2.2.4 Control Strategies for Cascade Systems

Performance optimization of cascade VCS relies on the coordinated control of expansion devices, compressors, and intermediate conditions. The expansion device regulates refrigerant mass flow and superheat, directly influencing system capacity and COP. The LS compressor speed significantly impacts the heat exchange between the two cycles; increasing LS speed raises cooling capacity but also raises the LS condensing temperature and thus raises the HS evaporator and condenser temperatures which increases power consumption, thereby reducing COP. The HS compressor speed also plays an important role by affecting the pressure ratios, refrigerant mass flow rates, and overall cooling capacity. While increasing HS speed increases cooling capacity, the associated power consumption rises more rapidly, ultimately lowering COP [8].

In addition, the intermediate temperature between the two stages serves as a key control variable. Studies have shown that setting the intermediate temperature as a real-time variable that depends on the LS evaporator and HS condenser temperatures improves COP and overall performance when the operating conditions are dynamic [12][13].

3
Model Setup

To study the behavior of a VCS under varying operating conditions, a model was developed in MATLAB Simscape. Simscape was chosen because it provides a component-based modeling approach that allows rapid prototyping of thermodynamic systems without requiring detailed implementation of governing equations. This makes it well-suited for exploring complex interactions and for testing control strategies.

The model development followed a stepwise approach. First, a simplified single-stage system was implemented to establish a working baseline and to gain familiarity with the modeling environment. Once this framework operated as expected, it was extended into a two-stage cascade configuration. Finally, control strategies were introduced to regulate critical system variables and enable evaluation of the system response under dynamic conditions.

The following sections describe each step in this process, starting with the single-stage cycle, followed by the two-stage cascade configuration, and concluding with the implementation of control loops.

3.1 Single-Stage VCS Model

The single-stage VCS, representing the LS of the cascade configuration, is designed to provide a cooling capacity of 25 kW while maintaining a liquid coolant temperature at 20 °C. This coolant serves as the heat-transfer medium between the electronics being cooled and the VCS.

3.1.1 Operating Point

The targeted operating point is defined based on the most demanding operating condition, corresponding to an HS ambient temperature of 100 °C combined with the maximum expected heat load of 25 kW. In this work, an *operating condition* refers to the combination of ambient temperature and heat load, which together define the thermal boundary constraints for the system. These constraints are particularly important since the HS condenser must reject heat to an elevated ambient temperature, which in turn raises the required LS condenser pressure and saturated temperature.

For the LS cycle, R134a was selected as the refrigerant due to its favorable thermodynamic properties within the targeted temperature range. Specifically, it provides pressures above the atmospheric pressure near the required evaporation temperature of 20 °C and can be condensed at elevated temperatures without excessive compressor pressure ratios. The resulting LS operating point is derived from a state point calculation of R134a using NIST REFPROP [14].

To ensure sufficient heat transfer across both the evaporator and condenser, an initial temperature difference of 10 °C is applied at the heat exchangers. The LS condenser saturation temperature is determined using the geometric mean between the LS evaporator and HS condenser saturation temperatures, yielding $T_{int} = 56.2\,°C$ when a HS condenser saturation temperature of 110 °C is assumed, using Equation (3.1).

$$T_{int} = \sqrt{T_{c,evap,sat} \cdot T_{h,cond,sat}} \tag{3.1}$$

To avoid wet compression and improve cooling performance, a superheat of 5 °C and a subcooling of 5 °C are applied. The required refrigerant mass flow rate is obtained from the energy balance:

$$\dot{m}_{ref} = \frac{\dot{Q}}{h_{evap,out} - h_{evap,in}}, \tag{3.2}$$

where $\dot{Q}$ is the desired cooling capacity. For R134a, the operating parameters are as follows:

- **Evaporator:** A saturated temperature of $T_{l,evap,sat} = 283.15\,K$ (10 °C) corresponding to a pressure of $p_{l,evap} = 0.41\,MPa$. Applying a superheat of 5 °C yields an evaporator outlet temperature of $T_{l,evap,out} = 288.15\,K$ (15 °C) and a specific enthalpy of $h_{l,evap,out} = 409\,kJ\,kg^{-1}$.
- **Condenser:** A saturated temperature of $T_{l,cond,sat} = 334.35\,K$ (61.2 °C) corresponding to a pressure of $p_{l,cond} = 1.73\,MPa$. With a subcooling of 5 °C, the condenser outlet temperature is $T_{l,cond,out} = 329.35\,K$ (56.2 °C) and the specific enthalpy is $h_{l,cond,out} = 281\,kJ\,kg^{-1}$.
- **Mass Flow Rate:** Using the above enthalpies, the required refrigerant mass flow rate is calculated to be $\dot{m}_{l,ref} = 0.20\,kg\,s^{-1}$ using Equation (3.2).

3.1.2 Initial Model

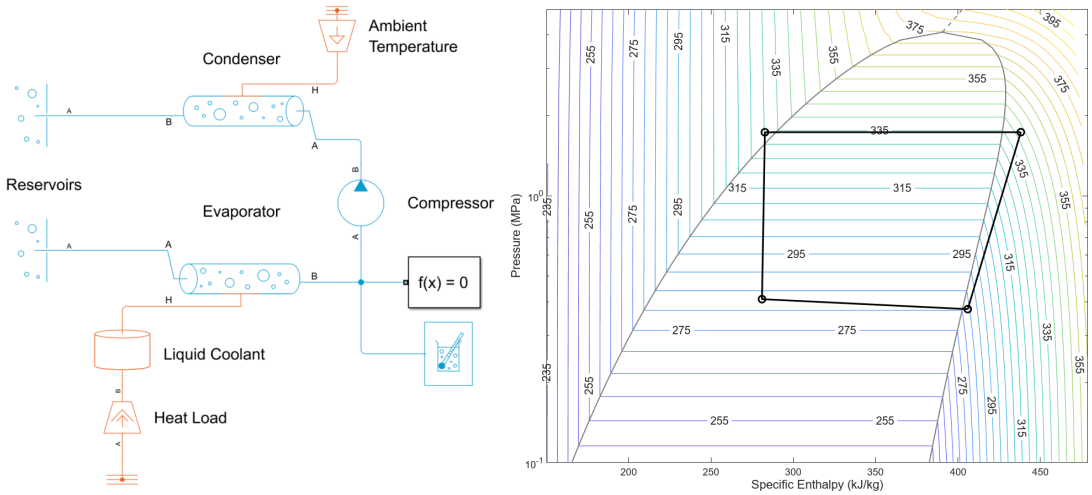

Figure 3.1: Initial single-stage VCS model connected to reservoirs for initialization, and the resulting *p*-*h* diagram.

The initial Simscape model of the single-stage VCS was constructed to verify the thermodynamic feasibility of the operating conditions derived in Section 3.1.1. The implemented configuration is shown in Figure 3.1. It consists of the following components:

- **Evaporator:** Modeled as a *Pipe (2P)* connected to a *Thermal Mass* representing 10 kg of a 10 % ethylene glycol–water mixture with a specific heat capacity of $4.189\,\mathrm{kJ\,kg^{-1}\,K^{-1}}$, simulating the liquid coolant. A *Heat Load Rate Source* applies a constant heat load of 25 kW.
- **Compressor:** Modeled as a *Flow Rate Source (2P)* delivering a constant refrigerant mass flow rate of $0.2\,\mathrm{kg\,s^{-1}}$, while performing isentropic work on the refrigerant.
- **Condenser:** Modeled as a *Pipe (2P)* connected to a fixed *Temperature Source* set to 51.2 °C.

To simplify initialization and guide the model toward the desired operating point, the evaporator inlet and condenser outlet were temporarily connected to two *Reservoir (2P)* components. These reservoirs were configured with fixed pressures and enthalpies corresponding to the calculated target conditions (Section 3.1.1). By imposing the correct boundary pressures, the model naturally settles into a steady-state solution without requiring accurate initial conditions or tuning of refrigerant charge. Once equilibrium is reached, the resulting outlet properties can be compared to the design targets to verify correct operation or determine if geometric adjustments are necessary. Furthermore, since the reservoirs control the outlet pressures, the expansion valve can remain disabled at this stage, simplifying the overall setup.

With this configuration, the evaporator and condenser dimensions were tuned to achieve the desired operating point. The resulting dimensions were:

- **Evaporator:** Length 100 m, cross-sectional area $1 \times 10^{-3}\,\mathrm{m}^2$, and hydraulic diameter $\frac{\sqrt{1e-3}}{\pi} \cdot 2 = 0.0357\,\mathrm{m}$, assuming a circular cross-section. These dimensions ensured sufficient heat transfer for the thermal mass to converge to approximately 20 °C.
- **Condenser:** Length 75 m, cross-sectional area $1 \times 10^{-3}\,\mathrm{m}^2$, and hydraulic diameter 0.0357 m, chosen to achieve the target condenser outlet enthalpy of $281\,\mathrm{kJ\,kg^{-1}}$.

The initial model successfully achieved the required cooling capacity of 25 kW. However, two limitations were observed. First, the temperature of the liquid coolant remains uniform at around 20 °C across the entire heat exchanger with this configuration. In a real system, a temperature gradient would develop along the flow direction as heat is absorbed, but the static thermal mass model failed to capture this behavior, resulting in an unrealistic representation of the heat transfer process. Second, the long evaporator length introduced a significant pressure drop caused by internal friction and turbulence, which reduced overall system efficiency.

3.1.3 Modified Design

To improve performance and achieve more accurate system behavior, the initial model was revised with updated components and refined operating conditions, as shown in Figure 3.2.

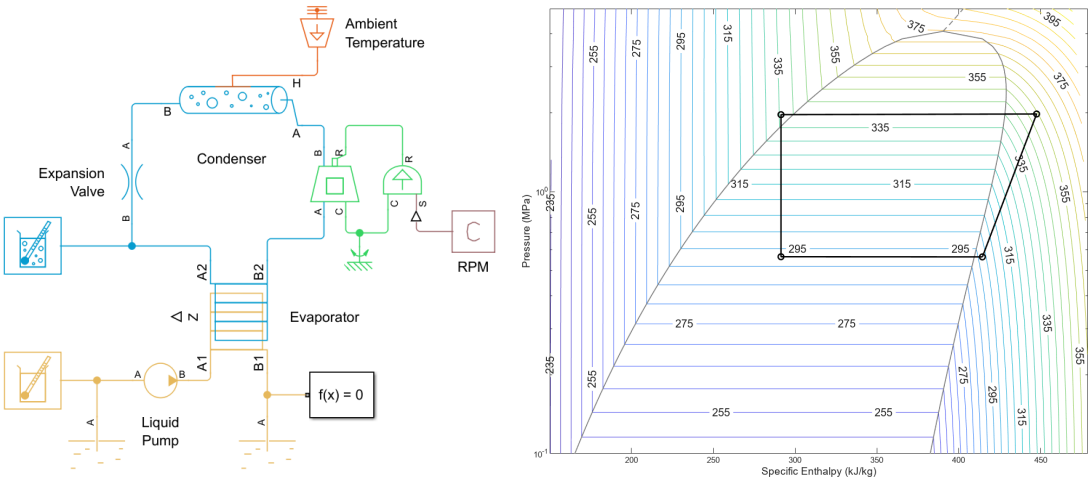

Figure 3.2: Modified single-stage VCS model implementing an expansion valve for closed-loop operation, along with the resulting *p-h* diagram.

The compressor used in the initial configuration was replaced with a *Positive-Displacement Compressor (2P)* that provides a nominal mass flow rate of $0.2\,\mathrm{kg\,s^{-1}}$ at a nominal shaft speed of 1000 rpm. An isentropic efficiency of 0.8 was applied to account for real-world compression losses, resulting in a more representative performance compared to the previous idealized model.

The evaporator was substituted with a *Plate Condenser Evaporator (TL-2P)*, a

Simscape component designed to model heat transfer between a two-phase refrigerant and a thermal liquid. This configuration uses a plate-type heat exchanger, which offers higher heat transfer coefficients, thereby improving system dynamics and reducing pressure drops. A counterflow arrangement was selected since it maximizes the overall heat transfer rate. The heat exchanger consists of 25 plates, each with a length of 1 m and a width of 0.5 m.

The evaporator is coupled to a thermal liquid network containing a 10 % ethylene glycol–water mixture representing the liquid coolant. Within this network, two thermal liquid reservoirs are used: one located at the evaporator inlet with a fixed temperature of 40 °C, and another acting as a thermal sink at the outlet. A flow rate source drives the coolant through the evaporator, where the mass flow rate $\dot{m}_{cool}$ is adjusted depending on the desired heat load. The goal is to maintain a coolant outlet temperature of 20 °C, with a nominal value of $0.3\,\mathrm{kg\,s^{-1}}$ corresponding to a reference heat load of 25 kW, based on the energy balance:

$$\dot{m}_{cool} = \frac{\dot{Q}}{c \cdot \Delta T}, \tag{3.3}$$

where $c = 4.189\,\mathrm{kJ\,kg^{-1}\,K^{-1}}$ for the mixture. This setup allows the model to evaluate system performance across varying heat loads.

In the initial model, the evaporator temperature difference was set to 10 °C, which caused excessive superheating at the evaporator outlet in the new setup, lowering overall efficiency. Since the coolant inlet temperature is relatively high at 40 °C, the evaporator temperature difference was reduced to 2 °C to obtain the desired operating point. This adjustment results in new operating parameters:

- **Evaporator:** A saturated temperature of $T_{l,evap,sat} = 291.15\,\mathrm{K}$ (18 °C) corresponding to a pressure of $p_{l,evap} = 0.54\,\mathrm{MPa}$. Applying a superheat of 5 °C yields an evaporator outlet temperature of $T_{l,evap,out} = 296.15\,\mathrm{K}$ (23 °C) and a specific enthalpy of $h_{l,evap,out} = 414\,\mathrm{kJ\,kg^{-1}}$.
- **Intermediate Temperature:** Calculated as the geometric mean between the LS evaporator and HS condenser saturation temperatures, giving $T_{int} = 334\,\mathrm{K}$ (60.85 °C).
- **Condenser:** A saturated temperature of $T_{l,cond,sat} = 339\,\mathrm{K}$ (65.85 °C) corresponding to a pressure of $p_{l,cond} = 1.92\,\mathrm{MPa}$. Applying 5 °C of subcooling yields a condenser outlet temperature of $T_{l,cond,out} = 334\,\mathrm{K}$ and a specific enthalpy of $h_{l,cond,out} = 288\,\mathrm{kJ\,kg^{-1}}$.
- **Mass Flow Rate:** The refrigerant mass flow rate is maintained at $\dot{m}_{l,ref} = 0.20\,\mathrm{kg\,s^{-1}}$ using Equation (3.2).

At this stage, the previously open system can be closed by introducing an expansion valve between the evaporator inlet and condenser outlet. A *Local Restriction (2P)* component is used for this purpose, with an experimentally determined opening area of $5.8 \times 10^{-6}\,\mathrm{m^2}$, obtained by iteratively adjusting the restriction until the desired pressure ratio was achieved. As described in Section 3.1.1, reservoir-based initialization is used to bring the system to a steady-state. Once the system reaches

steady-state, the resulting operating point is used as initial value for the closed system.

3.2 Extension to Two-Stage Cascade System

After verifying that the single-stage model operates as intended, the system can be extended into a two-stage cascade configuration. This approach allows the LS cycle to operate with R134a, while the HS uses R1233zd(E), since it enables condensation at ambient temperatures above 100 °C without reaching excessively high pressures. The HS is designed to reject approximately 33 kW of heat to the ambient environment, corresponding to the combined load of the LS evaporator and compressor power.The two stages are thermally coupled through an intermediate heat exchanger.

3.2.1 HS Operating Conditions

Based on the calculation of the state point for R1233zd(E) [14], the following conditions are defined:

- **Evaporator:** The evaporator operates at a saturated temperature of $T_{h,evap,sat} = 329\,\mathrm{K}$ (55.85 °C) and $p_{h,evap} = 0.35\,\mathrm{MPa}$. This value is based on an intermediate temperature of $T_{int} = 334\,\mathrm{K}$ reduced by 5 °C to ensure a 10 °C temperature difference in the heat exchanger. A superheat of 5 °C results in an evaporator outlet temperature of $T_{h,evap,out} = 334\,\mathrm{K}$ with an enthalpy of $h_{h,evap,out} = 447\,\mathrm{kJ\,kg^{-1}}$.

- **Condenser:** A saturated temperature of $T_{h,cond,sat} = 383.15\,\mathrm{K}$ (100 °C), corresponding to a pressure of $p_{cond} = 1.29\,\mathrm{MPa}$. With 5 °C of subcooling, the outlet temperature is $T_{h,cond,out} = 378.15\,\mathrm{K}$ (105 °C) and the specific enthalpy $h_{h,cond,out} = 334\,\mathrm{kJ\,kg^{-1}}$.

- **Mass Flow Rate:** The HS refrigerant mass flow rate is calculated to be $\dot{m}_{h,ref} = 0.30\,\mathrm{kg\,s^{-1}}$. using Equation (3.2).

3.2.2 System Configuration and Components

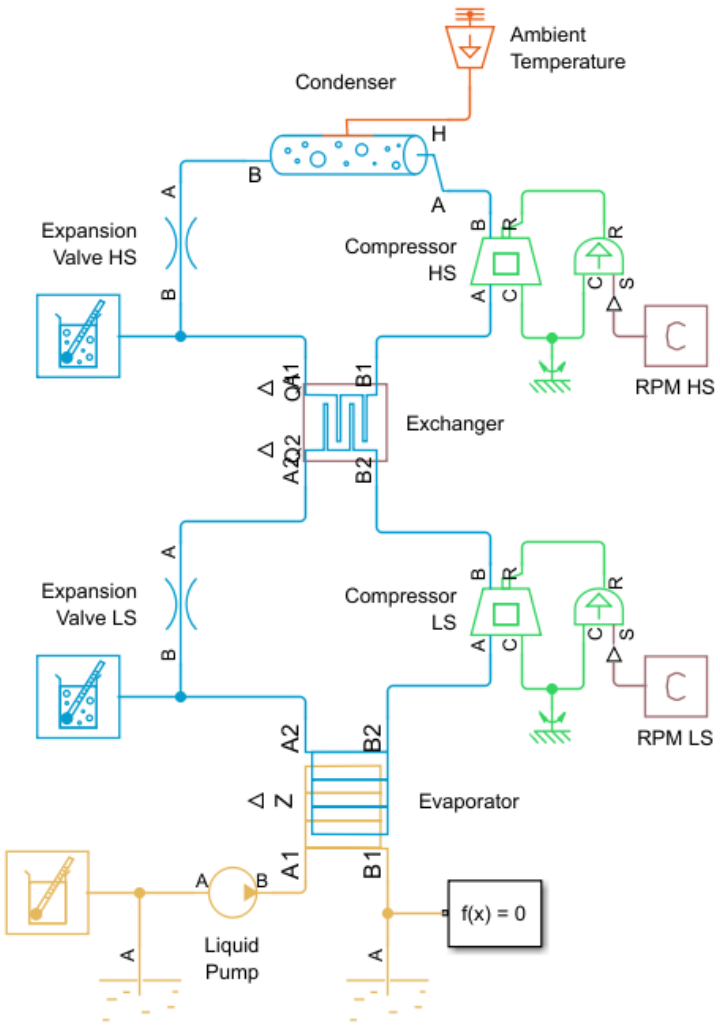

Figure 3.3: Full two-stage VCS model integrating the LS and HS cycles.

The two-stage cascade configuration integrates the LS and HS cycles, as illustrated in Figure 3.3. This design ensures efficient heat rejection and stable system operation by thermally coupling the stages while allowing each to operate at its optimal pressure and temperature levels.

- **System-Level Heat Exchanger (2P–2P):** The LS condenser and HS evaporator are thermally coupled using a *System-Level Heat Exchanger (2P–2P)*. This component models heat transfer between two two-phase refrigerant domains based on nominal operating performance data rather than geometrical details. The heat exchanger is parameterized using the operating conditions obtained from the LS and HS models.
- **HS Condenser:** A *Two-Phase Fluid (2P) Pipe* is used to model the condenser, configured similarly to the LS condenser but with a pipe length of

100 m to achieve the desired enthalpy at the outlet. The geometry ensures proper condensation at the operating pressures and avoids excessive pressure drops.

- **HS Compressor:** A *Positive-Displacement Compressor (2P)* is selected for the HS, configured for a nominal mass flow rate of $0.3\,\mathrm{kg\,s^{-1}}$ at a nominal shaft speed of 1000, with an isentropic efficiency of 0.8 to account for real-world compression losses.
- **HS Expansion Valve:** A *Local Restriction (2P)* component is used to control expansion on the HS side. Its opening area is set to $1 \times 10^{-5}\,\mathrm{m^2}$, determined experimentally to achieve the required pressure ratio during steady-state operation.

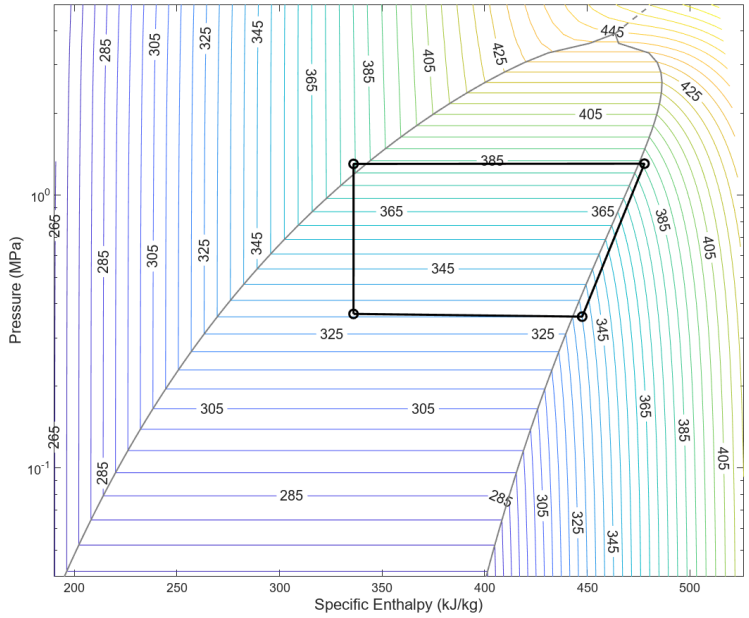

Figure 3.4: The resulting *p-h* diagram of the HS.

Similar to the single-stage model, the cascade system's initial conditions are generated by connecting reservoirs to the evaporator inlets and condenser outlets, bypassing the expansion valve. Figure 3.4 shows the *p-h* diagram of the HS.

3.3 Control Strategy

With the two-stage cascade model established, a control strategy is required to ensure stable and efficient operation under dynamic operating conditions, where both ambient temperatures and heat loads vary significantly. The objectives are to regulate the system for stable performance, protect components from unsafe operating conditions, and maximize overall cooling efficiency.

To achieve these objectives, Proportional-Integral (PI) controllers are implemented. Their role is to regulate key variables according to the following targets:

- Maintain a constant superheat of 5 °C for both LS and HS evaporators to ensure dry compression and prevent liquid slugging.

- Regulate the liquid coolant outlet temperature to 20 °C to meet thermal management requirements.
- Control the intermediate temperature to the geometric mean of the LS evaporator and HS condenser saturated temperatures, ensuring balanced compressor workloads.

This control framework builds on the methodology presented by Feng et al. [12] and Wang et al. [13], where the intermediate temperature is treated as a real-time variable, and on the findings of Jeong and Smith [11], which indicate that using the geometric mean as intermediate temperature provides optimal pressure ratios between stages, as mentioned in Section 2.2.1. While the geometric mean does not directly balance the compressor workload or maximize the COP, it serves as an effective and computationally efficient approximation for the true optimal intermediate temperature.

The PI controllers are tuned using MATLAB's Transfer Function-Based Tuning App at the highest expected load condition, defined by an ambient temperature of 383.15 K and coolant mass flow rate of $0.3\,\mathrm{kg\,s^{-1}}$. To smooth the control signals and eliminate algebraic loops in the simulations, a first-order transfer function of the form $G(s) = \frac{1}{s+1}$ is applied.

3.3.1 Superheat Control for Each Stage

Superheat is controlled independently for the LS and HS evaporators. The refrigerant temperature and the corresponding saturation temperature is measured at the evaporator outlet, and these values are compared against each other. The resulting value is compared against the setpoint of 5 °C, and the resulting error signal is fed into the PI controller. Figure 3.5 shows how the controls are implemented in the model. The PI output regulates the opening of the expansion valve to maintain the desired superheat. The expansion valve opening area is constrained between $1 \times 10^{-6}\,\mathrm{m^2}$ and $9 \times 10^{-4}\,\mathrm{m^2}$.

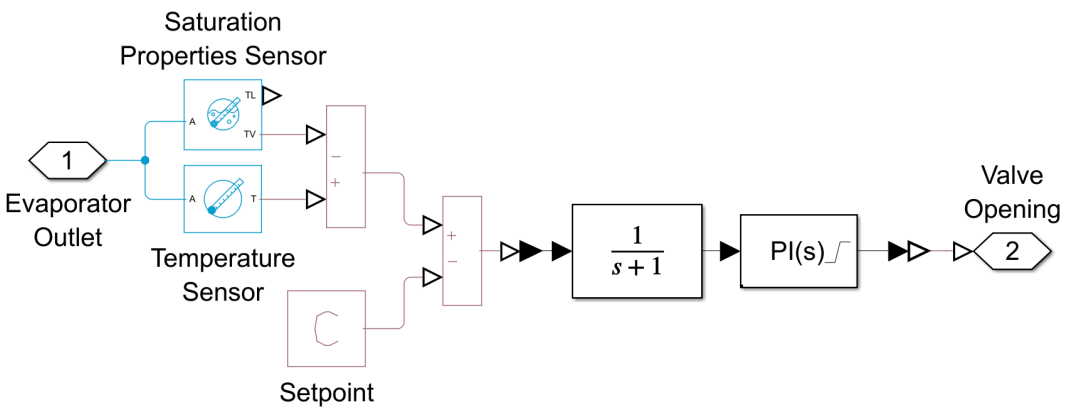

Figure 3.5: The implementation of the valve controls in the model.

3.3.2 LS Compressor Control for Engine Coolant Outlet Temperature

The LS compressor is responsible for maintaining the engine coolant outlet temperature at 20 °C. A Temperature Sensor located at the outlet of the evaporator measures the coolant temperature, which is compared against the setpoint. The resulting error is sent to a PI controller that modulates the LS compressor speed, thereby controlling the refrigerant mass flow rate to match the cooling demand. Figure 3.6 shows the implementation of the controller in the model. This approach ensures that the coolant remains within the required temperature range while minimizing unnecessary compressor power consumption.

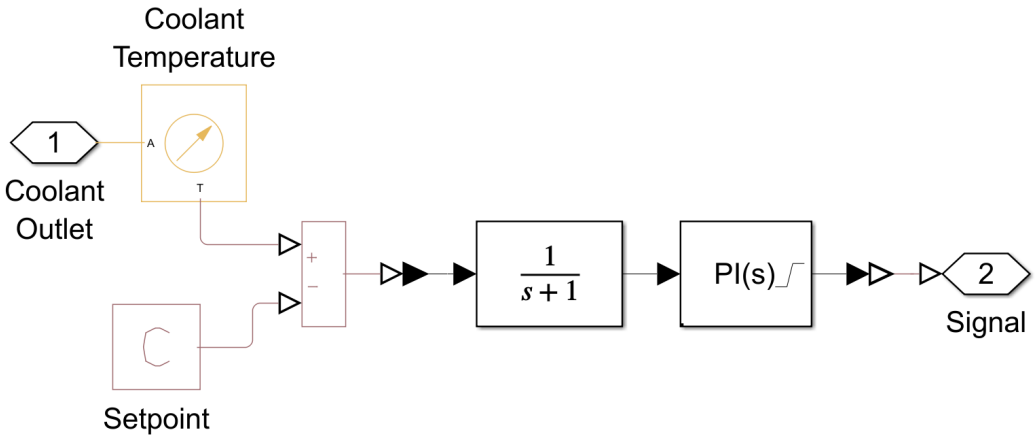

Figure 3.6: The implementation of the control for the LS compressor in the model.

3.3.3 HS Compressor Control for Intermediate Temperature

The HS compressor regulates the intermediate temperature T_{int} to balance the thermal loads between the two stages. The setpoint is defined as the geometric mean of the saturated temperatures of the LS evaporator and the HS condenser according to Equation (3.1). The arithmetic mean of the saturated temperature of the LS condenser and HS evaporator is used as process value:

$$T_{int,pro} = \frac{T_{c,cond,sat} + T_{h,evap,sat}}{2} \tag{3.4}$$

The intermediate temperature error, defined as the difference between T_{int} and $T_{int,pro}$, is minimized by adjusting the HS compressors speed. The implementation is shown in Figure 3.7. This control strategy ensures coordinated operation between the two stages, dynamically balancing refrigerant flows and pressure ratios under varying thermal loads while maintaining system stability and cooling efficiency.

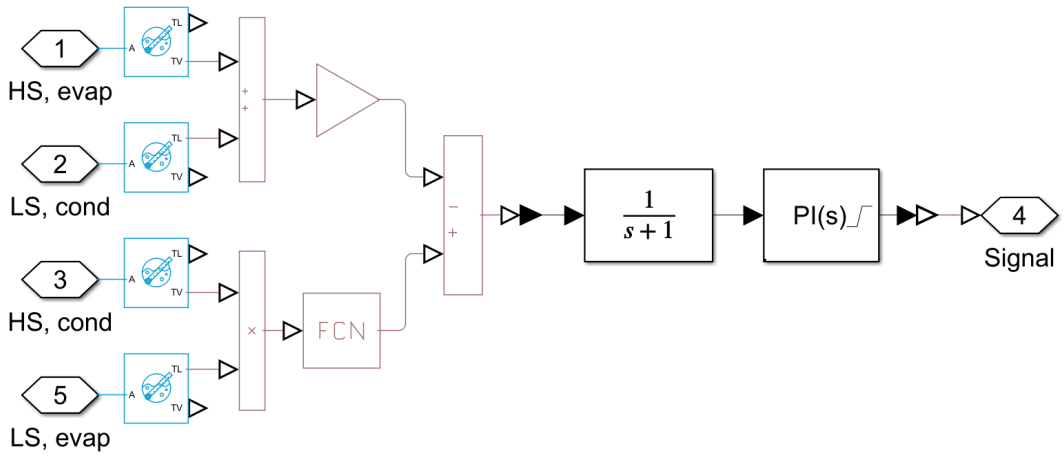

Figure 3.7: The implementation of the control for the HS compressor in the model.

4

Simulations and Results

This chapter presents the evaluation of the two-stage vapor compression system under varying operating conditions. The analysis follows a structured approach: first, the operating range of the model is determined to establish the conditions under which the system can operate without loss of stability. This provides an understanding of the boundaries where the controllers and cycle configuration are able to maintain target values.

Next, the system is subjected to step changes in key inputs, namely ambient temperature and coolant mass flow rate. These tests provide insight into the transient performance of the controllers, their ability to return system variables to their targets, and the corresponding adjustments in compressor speeds and expansion valve openings.

Finally, the system is evaluated under more realistic transient scenarios, which introduce gradual and coupled variations in operating conditions. In this stage, additional performance parameters such as COP and pressure ratios are examined, providing a broader view of how the system behaves in practice.

All simulations are carried out using the `daessc` solver, a differential-algebraic equation solver designed for physical systems with algebraic constraints. The solver is configured to use variable time steps, allowing accurate resolution of both slow thermal dynamics and rapid transients.

4.1 Working Range

The first set of simulations is designed to determine the operational limits of the VCS by progressively reducing ambient temperature and coolant liquid flow rates until the system reaches its limits. These limits include failure to converge toward target temperatures, inability to maintain the desired superheat, or failure to reach steady state in the simulation.

4.1.1 Ambient Temperature

The ambient temperature is decreased in steps of 1 °C every 1000 s from an initial value of 100 °C. The coolant mass flow rate remains constant at $0.3\,\mathrm{kg\,s^{-1}}$ throughout the simulation.

The coolant outlet and intermediate temperatures remain close to their respective targets across most of the ambient temperature range. At an ambient temperature of approximately 0 °C, both temperatures begin to oscillate around their targets, accompanied by oscillations in the LS and HS compressor speeds. The LS superheat gradually diverges from its nominal value when the ambient temperature falls below 7 °C, while the HS superheat remains close to its target until about 0 °C. The LS expansion valve opens progressively as the ambient temperature decreases and becomes fully open at 0 °C. In contrast, the HS valve remains relatively stable until approximately −1 °C, where it also opens fully.

4.1.2 Liquid Coolant Flow Rate

The flow rate of the liquid coolant is decreased in steps of $1\,\mathrm{g\,s^{-1}}$ every 1000 s from an initial value of $0.3\,\mathrm{kg\,s^{-1}}$. The ambient temperature is kept constant at 100 °C during the simulation.

As the coolant flow rate decreases, both the temperatures and the LS superheat deviate further from their targets, with oscillations of increasing amplitude and longer settling times. At $0.14\,\mathrm{kg\,s^{-1}}$, the system no longer reaches its target values within the 1000 s interval, with oscillations appearing in both compressors and both valves. At $0.10\,\mathrm{kg\,s^{-1}}$, the oscillation amplitude increases rapidly. The HS superheat remains close to its target until about $0.05\,\mathrm{kg\,s^{-1}}$, at which point it oscillated significantly and periodically dropped to 0 °C, indicating entry into the two-phase region. At this flow rate, the intermediate temperature also shows increased oscillation amplitudes. Additionally, the LS expansion valve reaches its closing limit of $1 \times 10^{-6}\,\mathrm{m^2}$, further constraining system stability.

4.1.3 Summary

From these simulations, the lower stability limit of the system was identified at approximately 7 °C ambient temperature under the baseline operating conditions of $0.30\,\mathrm{kg\,s^{-1}}$ coolant mass flow, and $0.10\,\mathrm{kg\,s^{-1}}$ coolant mass flow at 100 °C ambient temperature. Below these conditions, oscillations and loss of control prevent the system from reaching a steady state.

4.2 Step Response

This set of simulations evaluates the system's response to step changes in operation conditions by observing temperature deviations, compressor speeds, superheat behavior, and expansion valve openings.

4.2.1 Ambient Temperature

The ambient temperature was decreased in steps from 100 °C to 60 °C, then to 20 °C, before returning to 60 °C and finally 100 °C, with each step lasting 500 s. Simulations

were performed for two liquid coolant mass flow rates: $0.3\,\mathrm{kg\,s^{-1}}$ and $0.12\,\mathrm{kg\,s^{-1}}$.

4.2.1.1 Results at $\dot{m}_{cool} = 0.3\,\mathrm{kg\,s^{-1}}$

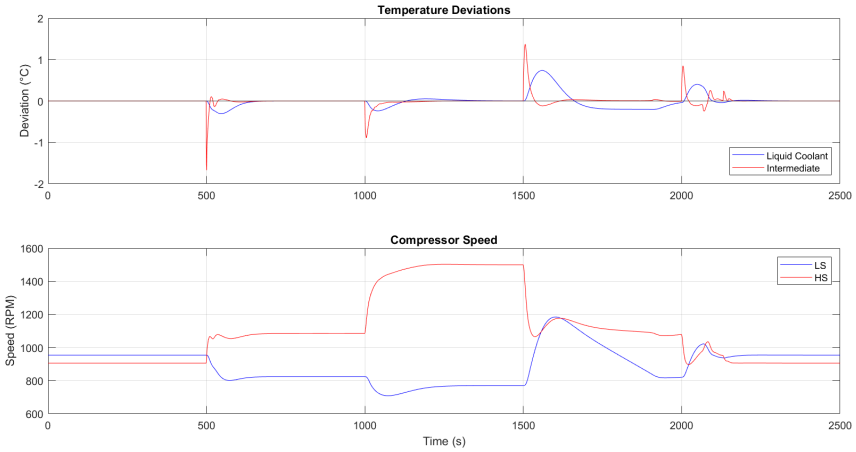

Figure 4.1: Temperature deviations and compressor speeds for ambient temperature step changes at $\dot{m}_{cool} = 0.3\,\mathrm{kg\,s^{-1}}$.

Figure 4.1 shows the temperature deviations for the coolant outlet and intermediate temperature, along with the LS and HS compressor speeds. At each ambient temperature step, the deviations exhibit sharp peaks that settle over time. The largest deviation is approximately 1.5 °C for the intermediate temperature and 0.7 °C for the coolant temperature. The LS compressor speed decreases as ambient temperature decreases, while the HS compressor speed increases.

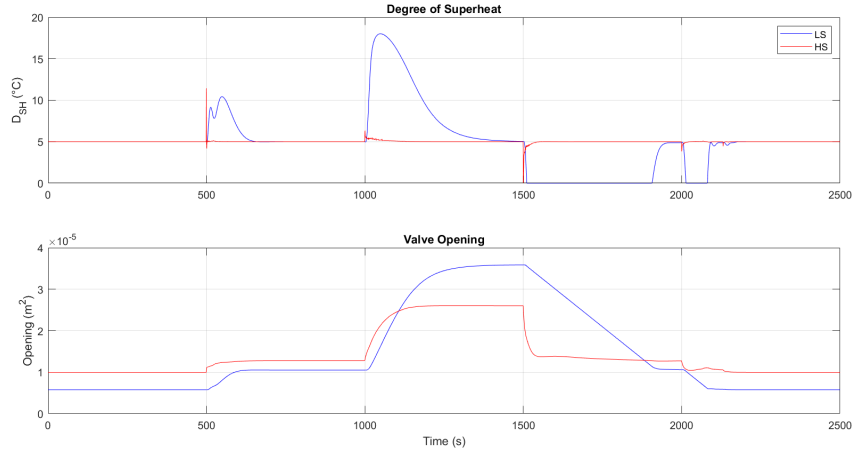

Figure 4.2: Superheat and expansion valve openings for ambient temperature step changes at $\dot{m}_{cool} = 0.3\,\mathrm{kg\,s^{-1}}$.

Figure 4.2 shows the LS and HS superheats together with the corresponding expansion valve openings. After each ambient temperature step, both LS and HS

superheats deviate from their target values, the HS superheat returns to its target level rapidly, while the LS superheat shows larger excursions and longer settling times. Notably, during the step increase from 20 °C to 60 °C, the LS superheat drops to 0 °C, indicating that the refrigerant enters the two-phase region and remains there for approximately 400 s before recovering.

4.2.1.2 Results at $\dot{m}_{cool} = 0.12\,\mathrm{kg\,s^{-1}}$

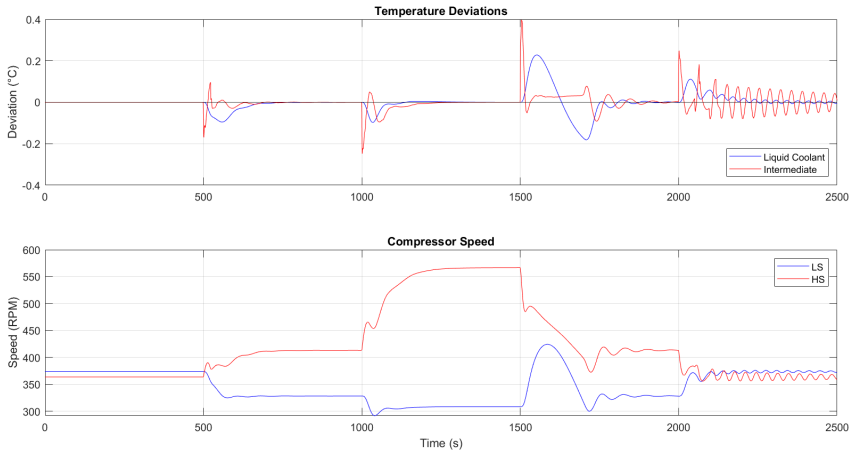

Figure 4.3: Temperature deviations and compressor speeds for ambient temperature step changes at $\dot{m}_{cool} = 0.12\,\mathrm{kg\,s^{-1}}$.

As shown in Figure 4.3, the behavior is similar to the case with $0.3\,\mathrm{kg\,s^{-1}}$, but with more pronounced oscillations after each step. After the step increasing the ambient temperature from 60 °C to 100 °C, the system shows persistent oscillations, especially the intermediate temperature and HS compressor speed, and does not return to the target within 500 s.

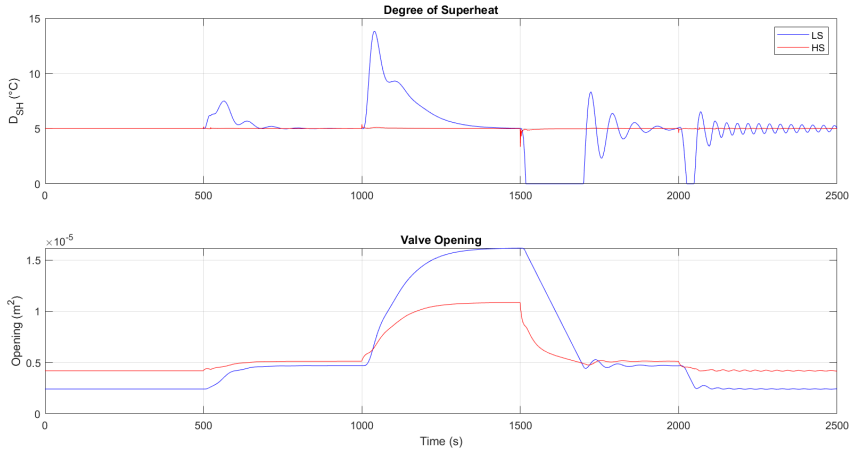

Figure 4.4: Superheat and expansion valve openings for ambient temperature step changes at $\dot{m}_{cool} = 0.12\,\mathrm{kg\,s^{-1}}$.

The LS superheat exhibits more oscillatory behavior compared to the case with $0.3\,\mathrm{kg\,s^{-1}}$, particularly during ambient temperature increases, as shown in Figure 4.4. At the final step from 60 °C to 100 °C, the LS superheat does not return to its targeted value within the simulated timeframe.

4.2.2 Liquid Coolant Flow Rate

The coolant mass flow rate was stepped from $0.3\,\mathrm{kg\,s^{-1}}$ to $0.2\,\mathrm{kg\,s^{-1}}$, then to $0.1\,\mathrm{kg\,s^{-1}}$, before returning to $0.2\,\mathrm{kg\,s^{-1}}$ and finally $0.3\,\mathrm{kg\,s^{-1}}$, with each step lasting 500 s. Two ambient temperatures were tested: 100 °C and 20 °C.

4.2.2.1 Results at $T_{\mathrm{amb}} = 100\,^{\circ}\mathrm{C}$

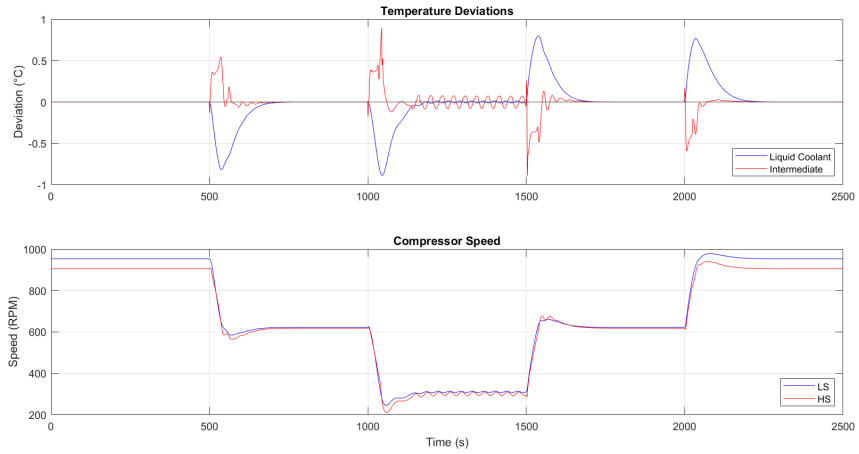

Figure 4.5: Temperature deviations and compressor speeds for coolant mass flow step changes at $T_{\mathrm{amb}} = 100\,^{\circ}\mathrm{C}$.

Figure 4.5 shows the temperature deviations and compressor speeds. At each flow rate step, the deviations exhibit short spikes that settle within approximately 200 s, except at $0.1\,\mathrm{kg\,s^{-1}}$, where the intermediate temperature shows continuous oscillations throughout the 500 s interval. These oscillations also occur for the HS compressor speed.

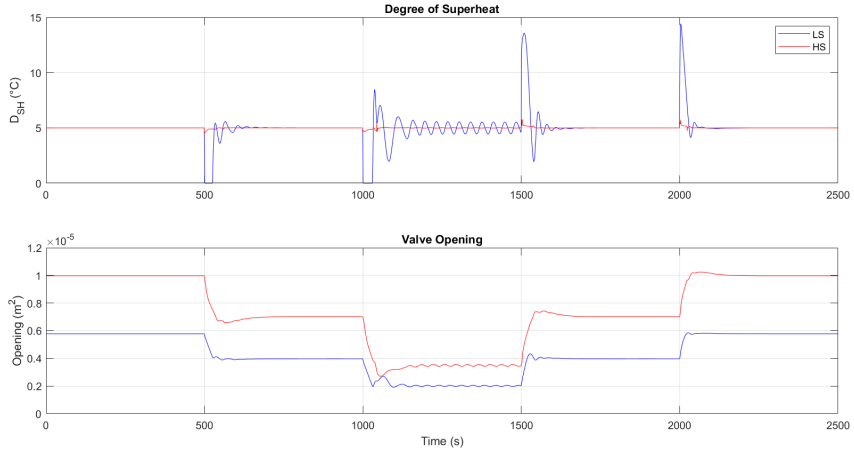

Figure 4.6: Superheat and expansion valve openings for coolant mass flow step changes at $T_{\text{amb}} = 100\,°\text{C}$.

The HS superheat remains close to its targeted value across all steps, whereas the LS superheat shows significant deviations after each step, as shown in Figure 4.6. At $0.1\,\text{kg}\,\text{s}^{-1}$, the LS superheat oscillates without returning to its targeted value during the entire interval. Oscillations also occur in both the LS and HS valve openings at that time.

4.2.2.2 Results at $T_{\text{amb}} = 20\,°\text{C}$

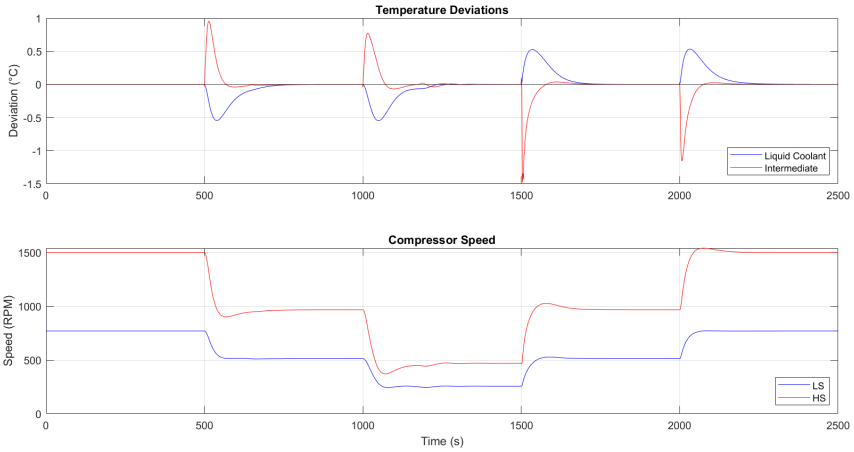

Figure 4.7: Temperature deviations and compressor speeds for coolant mass flow step changes at $T_{\text{amb}} = 20\,°\text{C}$.

As shown in Figure 4.7, the overall behavior is similar to the case at 100 °C, but the deviations return to their targets more gradually and with fewer oscillations. The temperatures also reaches their target within the 500 s interval at $0.1\,\text{kg}\,\text{s}^{-1}$ compared to the case of high ambient temperature.

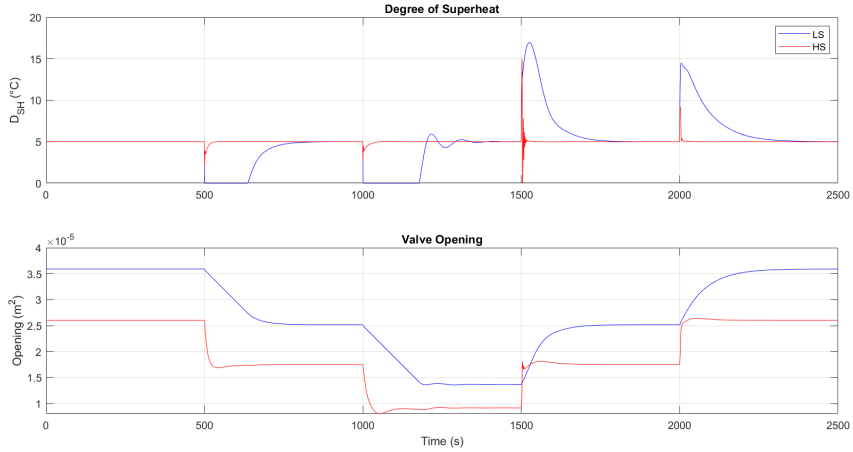

Figure 4.8: Superheat and expansion valve openings for coolant mass flow step changes at $T_{\text{amb}} = 20\,°\text{C}$.

Figure 4.8 shows the LS and HS superheats together with the corresponding expansion valve openings. The LS superheat behavior is similar to the 100 °C case, but deviations persist for a longer period after each step. Notably, the refrigerant persist in the two-phase region for roughly 200 s as the mass flow decreases. The HS superheat remains close to its nominal value but exhibits larger spikes compared to the high-ambient-temperature case.

4.3 Dynamic Scenarios

This simulation evaluates system performance under more realistic operating conditions, where both ambient temperature and coolant mass flow vary linearly rather than in discrete steps.

4.3.1 Input Signal

Figure 4.9 shows the applied input profiles for ambient temperature and coolant mass flow. The ambient temperature alternates between 100 °C and 20 °C using linear transitions of $0.1\,°\text{C}\,\text{s}^{-1}$. Independently, the coolant mass flow changes between $0.3\,\text{kg}\,\text{s}^{-1}$ and $0.1\,\text{kg}\,\text{s}^{-1}$ using linear transitions of $0.2\,\text{g}\,\text{s}^{-2}$. In the first part of the sequence, sequential combinations of high and low ambient temperatures and high and low mass flow rates are tested, with stable periods of 200 s at each level.

In the second part, both signals vary simultaneously. The ambient temperature maintains the same range of 100 °C to 20 °C, while the coolant mass flow alternates between $0.3\,\text{kg}\,\text{s}^{-1}$ and $0.14\,\text{kg}\,\text{s}^{-1}$. The signals start by simultaneously decreasing to the lower limit before increasing back up to the upper limit, combined with a 200 s at each extreme.

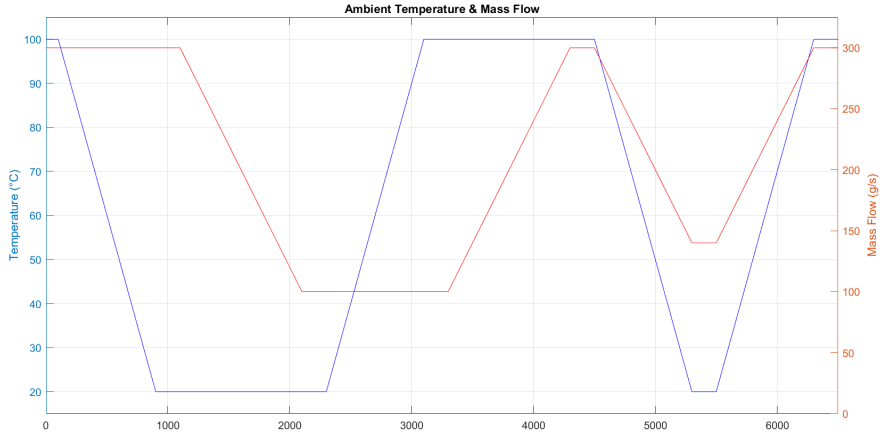

Figure 4.9: Input signals for ambient temperature and coolant mass flow rate.

4.3.2 Results

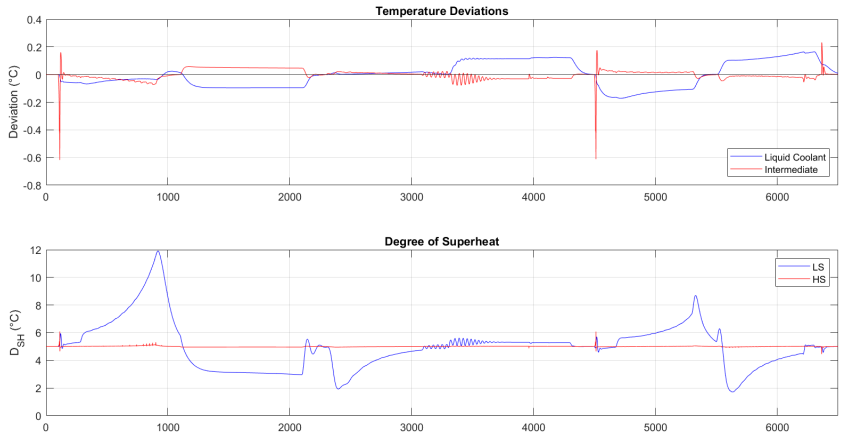

Figure 4.10: Temperature deviations and superheats for LS and HS.

Figure 4.10 shows the temperature deviations and the LS and HS superheats throughout the simulation. During transitions where the ambient temperature decreases, the intermediate temperature exhibits small spikes, but these settle rapidly. Overall, the temperatures remain close to their setpoints under all operating conditions, with small persistent errors observed for the coolant temperature. Regarding the superheats, the HS stays close to or at its target throughout the simulation, whereas the LS shows a persistent deviation during most of the simulation, peaking at around 12 °C when the ambient temperature decreases independently. When the ambient temperature begins increasing while the coolant mass flow is at its lower limit, both the intermediate temperature and LS superheat exhibit noticeable oscillations, similarly to Section 4.2.2.1.

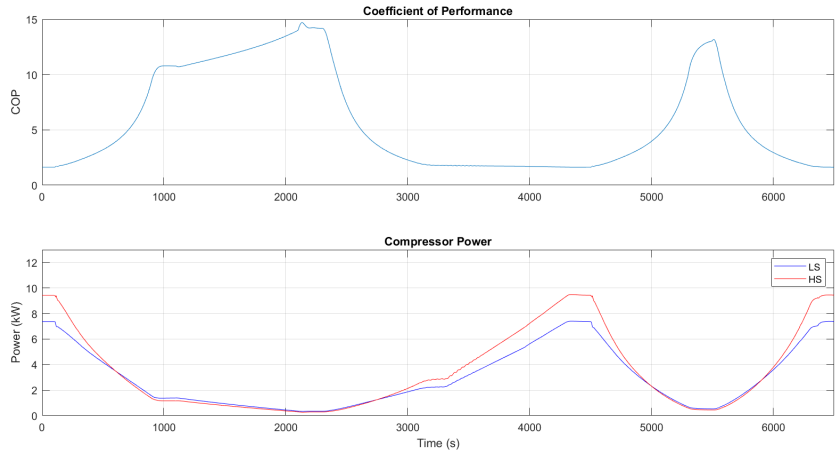

Figure 4.11: Coefficient of performance and compressor power consumption.

As shown in Figure 4.11, at the highest ambient temperatures, the COP is approximately 2 for both low and high mass flow rates. As the ambient temperature decreases, the COP increases and reaches nearly 15 under low-temperature, low-flow conditions. Compressor power decreases for both LS and HS when the ambient temperature drops. At higher ambient temperatures, the HS compressor consumes about 30% more power than the LS compressor. However, this difference diminishes as the coolant mass flow rate decreases.

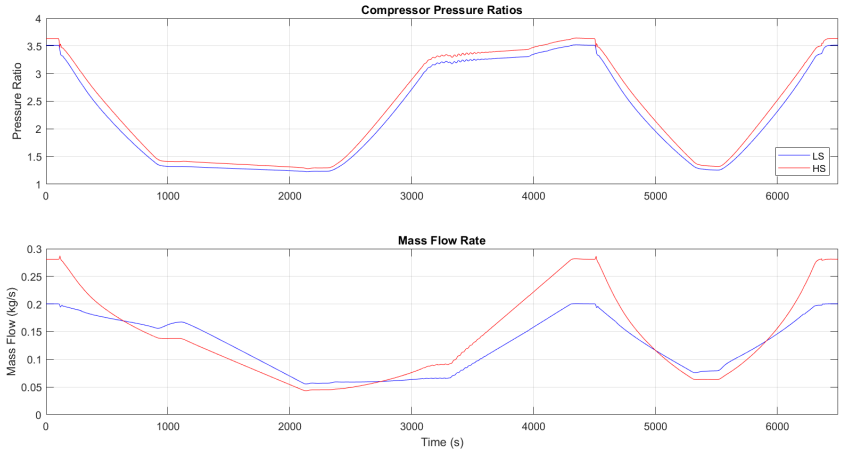

Figure 4.12: Compressor pressure ratios and mass flow rates for LS and HS.

Figure 4.12 shows the compressor pressure ratios and mass flow rates for both stages. The LS and HS pressure ratios remain close throughout the simulation, with the LS consistently lower by a small margin. These variations are primarily driven by changes in ambient temperature. In contrast, the LS and HS mass flow rates diverge more noticeably. At the most demanding operating point, the HS mass flow rate is approximately 40% higher than the LS. As the ambient temperature decreases under high coolant mass flow rates, the HS mass flow drops below that of the LS. Conversely, when the ambient temperature rises under low coolant mass flow rates,

the HS flow again exceeds the LS, indicating that the HS mass flow rate is more sensitive to ambient conditions.

5
Discussion

This chapter discusses the main findings of the study, interprets their implications, and relates them to the aims defined in Section 1.1. The results are also considered in light of the practical context of aerospace thermal management.

5.1 System Performance and Control Dynamics

The simulations demonstrated that the cascade VCS is capable of maintaining stable coolant temperatures across a broad range of operating conditions, including high ambient temperatures up to 100 °C. This indicates that a cascade configuration is suitable for handling large temperature lifts in aerospace environments where thermal loads can be high. The system consistently achieved coolant outlet temperatures close to their target values, with only minor persistent deviations.

At lower ambient temperatures, however, the system stability decreased. Below approximately 7 °C, oscillations in the coolant temperature, compressor speeds, and valve openings were observed. This behavior can be attributed to the evaporator and condenser pressures converge, reducing the effective pressure differential across the expansion valves and limiting their ability to regulate superheat.

The step response simulations provided insight into the dynamic behavior of the control system. For ambient temperature steps, the HS superheat returned to its target relatively quickly, while the LS superheat showed larger deviations and longer settling times. This difference could be a result of the HS evaporator pressure being directly coupled to the LS condenser, enabling faster adjustments, whereas the LS evaporator pressure depends primarily on the coolant temperature, making the response slower.

For coolant mass flow variations, the oscillations became increasingly severe at low flow rates. One possible contributor could be the solver step size, which may introduce oscillations in the results if too large. A more likely explanation, however, is that the oscillations arise from the controllers operating far from their tuning point, where the effective control gains became too large. A solution to this could be to employ gain scheduling or adaptive controllers to dynamically adjust control gains. More advanced strategies, such as multiple-input–multiple-output (MIMO) controllers, could also be investigated, particularly to coordinate compressor control.

Another notable observation was the opposite trend in compressor speeds under decreasing ambient temperatures. Section 4.2.1 shows that as the ambient temperature decreased, the HS compressor speed increased while the LS compressor speed decreased. Concurrently, Section 4.3.2 shows that lowering the ambient temperature led to reductions in mass flow rate and power input for both compressors. A possible explanation is that the HS condenser pressure drops with ambient temperature, which in turn lowers the LS condenser pressure and thereby reduces the required LS compressor workload. In contrast, the HS compressor is forced to operate at higher rotational speeds to sustain refrigerant circulation under the lower overall pressure levels in the HS cycle. The simultaneous reduction in mass flow rate and power input for both compressors suggests that the overall system demand decreases at low ambient conditions, even though the HS compressor must adjust its speed to maintain stable operation.

5.2 Energy Efficiency and Compressor Workload

The COP ranged from approximately 2 at high ambient temperatures to nearly 15 under low-temperature, low-load conditions. The lower values correspond to scenarios where substantial compressor work is required to overcome high pressure ratios, while the higher values arise when the ambient temperature is below the coolant inlet temperature, and only limited compression is needed to sustain refrigerant circulation and induce cooling.

The pressure ratios of the LS and HS compressors remained nearly identical across conditions, consistent with the use of the geometric mean for intermediate pressure regulation. However, the mass flow rates and power inputs of the compressors were not identical, with the HS compressor often consuming more power than the LS. This indicates that while the geometric mean balances pressure ratios, it does not perfectly distribute the workload. Further optimization of the intermediate pressure could therefore improve the COP of the system.

5.3 Strengths and Limitations of the Model

A key strength of the study is the demonstration that a cascade VCS can maintain stable cooling performance across a wide range of conditions. The results also show that the geometric mean is a robust approximation for the intermediate temperature, validating its use in system-level modeling.

At the same time, several limitations must be acknowledged. The model is highly idealized, with simplified representations of components and no consideration of gravitational or acceleration loads, which would affect refrigerant distribution in aerospace applications. Furthermore, the system did not remain stable at low ambient temperatures, a condition that is highly relevant for high-altitude flight.

An important practical observation concerns the system refrigerant charge and its implications for mass. The modeled system contains approximately 125 kg of refrigerant in total, with roughly 1.7 kg in the LS cycle and the remainder in the HS, concentrated almost entirely within the condenser. This large HS charge appears to be a consequence of the current HS condenser design as a uniform pipe rather than a more compact, multi-channel heat exchanger. It is difficult to quantify whether this affects the observed dynamic behavior from the simulations.

Finally, from a modeling perspective, the study is limited to simulation results, with no experimental validation to confirm the accuracy of the findings. Consequently, the observed dynamics may differ in a physical system, particularly due to unmodeled effects such as component tolerances, fluid distribution, and real heat exchanger performance.

5.4 Implications for Aerospace Applications

In aerospace contexts, weight and reliability are critical considerations. While this study did not explicitly account for component weight, practical systems would likely use compact heat exchangers with higher temperature differences to reduce size and mass, at the cost of increased compressor work.

Estimating the complete system mass in a practical implementation is challenging without component-level designs and structural details. Nevertheless, the magnitude of the refrigerant charge is a clear concern for aerospace application where weight and charge minimization are critical.

Another important limitation is the system's inability to operate at low ambient temperatures. This is particularly relevant for aerospace applications, where high-altitude conditions often involve sub-zero ambient temperatures. It should be noted that this behavior is inherent to VCSs operating below their design evaporator temperatures and is unlikely to be mitigated through control strategies.

5.5 Future Work

Building on the present work, several directions for future research can be identified:

- Implementing advanced control strategies, such as gain scheduling or MIMO controllers, to improve transient stability and robustness.
- Optimizing the intermediate pressure regulation beyond the geometric mean to achieve better workload distribution between compressors.
- Validating the simulations against experimental test rigs to confirm accuracy and practical feasibility.

6
Conclusion

The objective of this thesis was to investigate the performance and control of a two-stage cascade VCS under varying operating conditions, with a focus on aerospace applications. The simulations show that the cascade VCS is capable of maintaining stable coolant temperatures and achieving reasonable COP across a wide range of conditions. The use of the geometric mean for the intermediate pressure proved effective in balancing pressure ratios between stages, though discrepancies in compressor power inputs suggest that further optimization is possible.

At the same time, the study highlights important limitations. The system was unable to maintain stable operation at ambient temperatures below approximately 7 °C, which is a significant concern given that aerospace environments often expose systems to sub-zero conditions. Furthermore, the model neglects physical effects such as gravitational and acceleration loads, and its results have not yet been validated experimentally.

Future work should therefore focus on refining the control strategy, for example through adaptive or MIMO controllers, improving intermediate temperature regulation, and validating the model against experimental data. Addressing these challenges will be critical to advancing cascade VCS technology toward practical integration in next-generation aerospace thermal management systems.

Bibliography

[1] M. J. Moran, H. N. Shapiro, D. D. Boettner, and M. B. Bailey, *Fundamentals of Engineering Thermodynamics* 9th ed. Hoboken, NJ, USA: Wiley, 2018.

[2] V. P. S. Negi, C. Ranganayakulu, "Thermodynamic performance of three-wheel bleed and bleedless air cycle refrigeration systems for a commercial airliner environmental control system (ECS)," International Communications in Heat and Mass Transfer, vol. 159, Dec. 2024, doi: 10.1016/j.icheatmasstransfer.2024.108235.

[3] H. Zhang, Q. Wu, S. Feng, S. Dong, and Z. Gao, "Vapor Compression Refrigeration System for Aircrafts: Current Status, Large-Temperature-Range Challenges and Emerging Auto-Cascade Refrigeration Technologies," Aerospace, vol. 12, no. 8, Jul. 2025, doi: 10.3390/aerospace12080681.

[4] N. Jain and A. G. Alleyne, "Thermodynamics-based optimization and control of vapor-compression cycle operation: Optimization criteria," in *Proceedings of the American Control Conference,* 2011, pp. 1352 - 1357, doi: 10.1115/DSCC2011-6088.

[5] Y. A. Cengel, M. A. Boles and M. Kanoğlu, *Thermodynamics: An Engineering Approach*, 9th ed. New York, NY, USA: McGraw-Hill Education, 2019.

[6] H.M. Getu and P.K. Bansal, "Thermodynamic analysis of an R744–R717 cascade refrigeration system," International Journal of Refrigeration, vol. 31, no. 1, Jan. 2008, pp. 45-54, doi: 10.1016/j.ijrefrig.2007.06.014.

[7] V. Jain, S.S. Kachhwaha, G. Sachdeva, "Thermodynamic performance analysis of a vapor compression–absorption cascaded refrigeration system," Energy Conversion and Management, vol. 75, Nov. 2013, pp. 685-700, doi: 10.1016/j.enconman.2013.08.024.

[8] S. Boahen and J. M. Choi, “Research trend of cascade heat pumps,” Sci. China Technol. Sci., vol. 60, no. 11, pp. 1597-1615, Sep. 2018, doi: 10.1007/s11431-016-9071-7.

[9] A. Goyal, M. A. Staedter, S. Garimella, "A review of control methodologies for vapor compression and absorption heat pumps," International Journal of Refrigeration, vol. 97, pp. 1-20, Jan. 2019, doi: 10.1016/j.ijrefrig.2018.08.026.

[10] D. H. Kim, H. S. Park, M. S. Kim, "Optimal temperature between high and low stage cycles for R134a/R410A cascade heat pump based water heater system," Experimental Thermal and Fluid Science, vol. 47, pp. 172-179, Jan. 2013, 10.1016/j.expthermflusci.2013.01.013.

[11] S. Jeong, J.L. Smith, "Optimum temperature staging of cryogenic refrigeration system," Cryogenics, vol. 34, no. 11, pp. 929-933, 1994, doi: 10.1016/0011-2275(94)90078-7.

[12] Y. Feng, J. Shu, C. Wang, D. Ren, Z. Xing, L. Li, L. Liu, "Energy-saving control method for NH3-CO2 cascade refrigeration system by directly regulating slide valve position in twin-screw compressor," Applied Thermal Engineering, vol. 239, Feb 2024, 10.1016/j.applthermaleng.2023.122116.

[13] W. Wang, Q. Zhou, G. Tian, B. Hu, Y. Li, F. Cao, "The intermediate temperature optimization for cascade refrigeration system and air source heat pump via extreme seeking control," International Journal of Refrigeration, vol. 117, pp. 150-162, Sep. 2020, doi: 10.1016/j.ijrefrig.2020.05.007.

[14] E. W. Lemmon, I. H. Bell, M. L. Huber, M. O. McLinden, 2018, NIST Standard Reference Database 23, Version 9.5, National Institute of Standards and Technology, doi: 10.18434/T4/1502528.

DEPARTMENT OF SOME SUBJECT OR TECHNOLOGY
CHALMERS UNIVERSITY OF TECHNOLOGY
Gothenburg, Sweden
www.chalmers.se

CHALMERS
UNIVERSITY OF TECHNOLOGY